Analysis of Crowded Field Adaptive Optics Image Data

Matthew C. Britton

California Institute of Technology, Pasadena, CA 91125 USA

ABSTRACT

A point source deconvolution technique is described that models the effects of anisoplanatism on the adaptive optics point spread function. This technique is used in the analysis of a quadruple system observed using the Palomar Adaptive Optics system on the Hale 5 meter telescope. Two members of this system reside in a .1 asec double. Deconvolution of this close double was performed using the PSF of a third member of the system, which was offset from the double by 12 asec. Incorporation of anisoplanatism into the deconvolution procedure requires knowledge of the turbulence profile, which was measured at the time of these observations using a DIMM/MASS unit at Palomar Observatory.

1. INTRODUCTION

An adaptive optics (AO) system can provide tremendous benefits in angular resolution for near infrared image data. Observations of fields such as clusters and tight binaries in which there is overlap in the point spread function of adjacent stars benefit from this angular resolution. The reduction of these observations presents significant challenges, which arise from the complex evolution of the adaptive optics point spread function (PSF). The turbulence profile above a telescope can evolve on timescales of minutes, leading to a change in image quality delivered by the AO system and an evolution in the PSF obtained in the observation. This variability impacts the photometric and astrometric measurement accuracy.

A number of deconvolution techniques have been developed to perform photometric and astrometric analysis of AO compensated images that suffer from confusion.[1-3] These techniques use a model of the scientific target to establish a merit function, whose minimization yields the modeled parameters of the observation. For example the science target may consist of a number of point sources that are modeled as shifted and scaled copies of the PSF. In these techniques, an estimate of the PSF may be taken from an isolated point source in the image. Alternatively, the PSF may be derived as part of the deconvolution procedure if no such point source is available.

Another difficulty that arises in the analysis of AO image data lies in the field dependence displayed by the PSF, which arises from anisoplanatism. This effect is induced by the shear between columns of turbulent atmosphere traversed by light from the guide star and from an off axis science target. The AO system acts to compensate the guide star wavefront, and this correction decorrelates with increasing angular offset from the guide star. This degrades the image quality of the science target. The effects of anisoplanatism change in response to temporal evolution of the atmospheric turbulence profile, leading to both time and field dependence of the AO PSF. This induces substantial evolution in the image quality on minute timescales and over arcminute fields in the near infrared. The Strehl ratio may vary by factors of several at any particular point in the field, and by an order of magnitude or more across the field.

The anisoplanatic evolution of the AO PSF complicates the application of deconvolution algorithms. Because of this effect, a reference point source at one location in the field may be a poor representation of the PSF elsewhere in the field. In addition, the probability of finding such a reference grows with field size, while the fidelity of the reference PSF degrades with increasing angular offset from the guide star. Similarly, extraction of a PSF from the deconvolution procedure is complicated by the anisoplanatic field dependence, which was not modeled in the techniques cited above. These complications have limited the application of deconvolution algorithms to fields of order several arcseconds, over which the PSF may be assumed to be constant.

Recently, an analytic formulation has been developed that accounts for the effects of anisoplanatism on the adaptive optics PSF.[4] The results presented here describe a method in which this analysis is incorporated into a

---

Further author information: Send correspondence to Matthew Britton: E-mail: mbritton@astro.caltech.edu

deconvolution algorithm, thereby permitting deconvolution to be applied over much wider fields. This technique is applied to an observation of a quadruple system, in which two of the members reside in a .1 asec double. Section 2 describes the formulation of a crowded field point source model that accounts for anisoplanatism, while Section 3 describes the deconvolution procedure. Sections 4 and 5 describe the observations and the results of the experiment.

2. A CROWDED FIELD MODEL

Consider an adaptive optics observation of a number P of point sources distributed over a finite field of view. Due to the effects of anisoplanatism, the point spread function delivered by the adaptive optics system varies with angular offset from the guide star. The observation $i(\vec{\theta})$ may be modeled as the sum over a point spread function at the location of each source multiplied by a scaling factor to account for the source intensity.

$$i(\vec{\theta}) = \sum_{p=1}^{P} b_p r_p(\vec{\theta} + \vec{\theta}_p) \tag{1}$$

Here the subscript p labels each point source in the image, b_p is the intensity, $\vec{\theta}_p$ is the angular offset from the guide star, and $r_p(\vec{\theta})$ is the point spread function (PSF) at this angular offset. In this equation the guide star has been assumed to lie at the origin.

In the analysis to follow, the model in Equation 1 is more readily applied in the Fourier domain. In this domain, the angular offset $\vec{\theta}_p$ induces a phase gradient via the shift theorem.[5] The PSF and the optical transfer function (OTF) form a Fourier transform pair, so that in the Fourier domain Equation 1 becomes a sum over the OTFs of each point source. These OTFs depend on field location, and may be written as the product of two terms.[4, 6]

$$OTF(\vec{r}) = OTF_{gs}(\vec{r}) * ATF(\vec{r}) \tag{2}$$

Here $\vec{r}$ is a vector in the aperture plane, $OTF_{gs}(\vec{r})$ is the optical transfer function of the guide star and $ATF(\vec{r})$ is a transfer function that represents the effects of anisoplanatism. This latter term takes the form

$$ATF(\vec{r}) = \exp\left\{ -\frac{1}{2} D_{\mathrm{apl}}(\vec{r}) \right\} \tag{3}$$

The anisoplanatic structure function $D_{\mathrm{apl}}(\vec{r})$ may be written as an integral along the line of sight to the guide star as

$$D_{\mathrm{apl}}(\vec{r}) = 2\Xi k^2 D^{5/3} \int_0^\infty dz\, C_n^2(z) \left\{ 2\left|\vec{\Omega}_p\right|^{5/3} + 2\left|\frac{2\vec{r}}{D}\right|^{5/3} - \left|\frac{2\vec{r}}{D} + \vec{\Omega}_p\right|^{5/3} - \left|\frac{2\vec{r}}{D} - \vec{\Omega}_p\right|^{5/3} \right\} \tag{4}$$

Here k is the wavenumber, D is the aperture diameter, z is the range variable to the guide star, $\vec{\Omega}_p = 2z\vec{\theta}_p/D$ and the constant $\Xi = .458986$. The function $ATF(\vec{r})$ depends on observing wavelength, aperture diameter, the angular offset from the guide star $\vec{\theta}_p$, zenith angle, and the turbulence profile $C_n^2(z)$.

By taking the Fourier transform of Equation 1 and applying Equation 2, the transform $I(\vec{r})$ of the observation may be modeled as the product of $OTF_{gs}(\vec{r})$ with a sum over anisoplanatic transfer functions, each multiplied by a phase gradient to account for the angular offset from the guide star.

$$I(\vec{r}) = OTF_{gs}(\vec{r}) \sum_{p=1}^{P} b_p ATF_p(\vec{r}) \exp\left\{ i\, \vec{\theta}_p \cdot \vec{r} \right\} \tag{5}$$

This model is used in the analysis below.

3. FITTING THE OBSERVATIONS

To extract the amplitudes b_p and offsets $\vec{\theta}_p$ of each point source in the observation, define a χ^2 metric as

$$\chi^2 = \frac{1}{2\sigma^2} \int d\vec{r} \left| I(\vec{r}) - OTF_{gs}(\vec{r}) \sum_{p=1}^{P} b_p ATF_p(\vec{r}) \exp\left\{ i\,\vec{\theta}_p \cdot \vec{r} \right\} \right|^2 \tag{6}$$

In this expression, χ^2 is a function of the amplitude b_p, offset $\vec{\theta}_p$, and anisoplanatic transfer function $ATF_p(\vec{r})$ of each of the P point sources in the image, as well as the guide star optical transfer function $OTF_{gs}(\vec{r})$.

Iterative deconvolution algorithms converge much faster if the search starts at a point in parameter space that is nearly optimal. Initial estimates for b_p and $\vec{\theta}_p$ may be extracted from the observation itself. The latter are readily obtained to an accuracy of about a pixel, and $ATF_p(\vec{r})$ changes very little over these angular scales. Therefore, the initial estimates for $\vec{\theta}_p$ may be used to compute $ATF_p(\vec{r})$ at the outset of the fit. There are considerable practical difficulties in fitting directly for $OTF_{gs}(\vec{r})$, since this introduces a large number of degrees of freedom into the model. Instead, one may use an initial estimate for this function. One possibility is to use the idealized OTF that would be obtained in the absence of atmospheric turbulence. Another option is to form an OTF by extracting a point source directly from the observed data. This point source need not be the guide star itself, as an estimate of $OTF_{gs}(\vec{r})$ may be computed from the OTF of an off axis star using Equation 2. As will be shown below, it is straightforward to refine the initial estimate of $OTF_{gs}(\vec{r})$ using the parameters derived in the deconvolution.

With these assumptions, Equation 6 may be considered a function of the parameters b_p and $\vec{\theta}_p$. Since χ^2 is a nonlinear function of $\vec{\theta}_p$, minimization of χ^2 must be carried out iteratively. The derivatives of χ^2 with respect to b_p and $\vec{\theta}_p$ are

$$\nabla_{\vec{\theta}_p} \chi^2 = \frac{b_p}{\sigma^2} \int d\vec{r}\, \vec{r}\, \mathrm{Im}\left[G_p(\vec{r}) \right]$$

$$\frac{\partial \chi^2}{\partial b_p} = \frac{1}{\sigma^2} \int d\vec{r}\, \mathrm{Re}\left[G_p(\vec{r}) \right]$$

where

$$\begin{aligned} G_p(\vec{r}) = {} & ATF_p(\vec{r}) \exp\left\{ i\,\vec{\theta}_p \cdot \vec{r} \right\} \sum_q b_q ATF_q(\vec{r}) \exp\left\{ -i\,\vec{\theta}_q \cdot \vec{r} \right\} - \\ & OTF_{gs}(\vec{r}) \sum_q b_q ATF_q(\vec{r}) \exp\left\{ -i\,\vec{\theta}_q \cdot \vec{r} \right\} \end{aligned} \tag{7}$$

The set of values for b_p and $\vec{\theta}_p$ that minimize χ^2 may be determined iteratively using standard numerical techniques.[7]

Having determined the optimal values of b_p and $\vec{\theta}_p$, one may refine the estimate of $OTF_{gs}(\vec{r})$ by using Equation 5.

$$OTF_{gs}(\vec{r}) = I(\vec{r}) * \left[\sum_{p=1}^{P} b_p ATF_p(\vec{r}) \exp\left\{ i\,\vec{\theta}_p \cdot \vec{r} \right\} \right]^{-1} \tag{8}$$

The denominator on the right hand side of this expression incorporates information from the parameters derived in the deconvolution to coherently phase each of the OTFs that are present in the observation. In this way, noise in the estimate of $OTF_{gs}(\vec{r})$ should be substantially suppressed. The fit for b_p and $\vec{\theta}_p$ may be repeated using this refined estimate, if necessary. The resulting values for the fitted parameters may be used to construct a model for the observation from Equation 5. This model may then be compared directly to the observation.
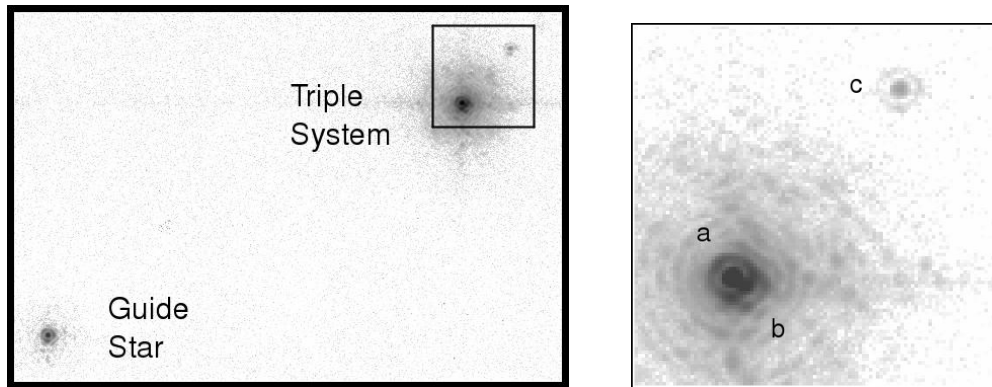
Figure 1. A 2.12 μm, 1.4 second exposure of HD206267 and its companion BD+56 2617C, shown on a log stretch. On the left panel a 14 x 9.4 asec subimage of the 25 square asec PHARO field is shown. BD+56 2617C was used as the guide star for the Palomar Adaptive Optics system PALAO and appears in the lower left corner of the image, while HD206267 appears in the upper right. The right panel shows a 2.5 square asec subfield containing HD206267. The image illustrates that this star is in fact a close double. A third, faint object is also visible towards the upper right corner of this panel. This object is itself a candidate companion to HD206267.

4. OBSERVATIONS

As an application of the technique above, adaptive optics observations of the system HD206267 + BD+56 2617C were carried out on the Hale 5 meter at Palomar Observatory on July 4, 2005. These stars have an angular separation of 12 asec, with magnitudes $m_v = 5.6$ and 8.3, respectively. The fainter of the two objects - BD+56 2617C - was used as the guide star for the Palomar Adaptive Optics system (PALAO),[8] while a 1.4 second exposure was acquired using the infrared camera PHARO.[9] These observations were performed at a wavelength of 2.123 μm using an H2 filter with a bandpass of .007 μm.

An observation of this field is shown in Figure 1, and illustrates that HD206267 is itself a double with angular separation of .1 asec. A third source is evident at an angular separation of 1.8 asec, and is also a candidate companion to HD206267. Measurement of the differential photometry and astrometry of the .1 asec double presents a challenge due to the large degree of PSF overlap. In fact, the companion sits directly upon the Airy ring of the primary. The formalism described in Sections 2 and 3 may be used to perform such a measurement.

Evaluation of the anisoplanatic transfer function requires a knowledge of the turbulence profile. For this experiment, measurements of $C_n^2(z)$ were carried out using a set of turbulence monitoring equipment composed of a Differential Image Motion Monitor (DIMM)[10] and a Multiaperture Scintillation Spectrometer (MASS).[11] This equipment was installed at Palomar Observatory as part of the Thirty Meter Telescope site testing program.[12] At the time of the observation in Figure 1, the Fried parameter and isoplanatic angle computed from the measured turbulence profile had values of $r_0 = 12$ cm and $\theta_0 = 3.1$ asec. These values are quoted at a reference wavelength of .5 μm.

With this measurement of $C_n^2(z)$, the anisoplanatic transfer functions may be evaluated from Equation 3 for each of the three targets HD206267a-c. The guide star BD+56 2617C provides a convenient PSF reference from which $OTF_{gs}(\vec{r})$ may be computed. These quantities were used together with initial estimates of b_p and $\vec{\theta}_p$ to model the observation using Equation 5. An iterative fit for the values of b_p and $\vec{\theta}_p$ for all four objects was then performed using the formalism in Section 3.

5. RESULTS

The amplitude of $I(\vec{r})$ computed from a Fourier transform of the observation is shown in Figure 2. This function is a superposition of four complex optical transfer functions, and displays ringing that arises from this superposition. For comparison the OTF amplitude for a single point source in the absence of atmospheric turbulence is also
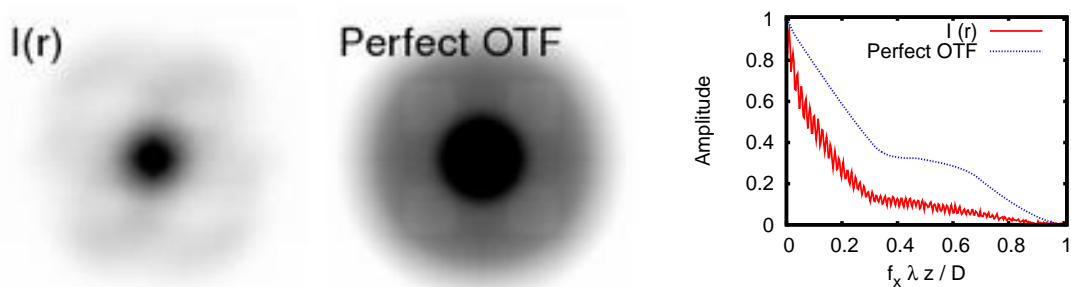
Figure 2. Amplitudes of the perfect optical transfer function and the transform $I(\vec{r})$ of the observation in Figure 1. The left and center panel show these functions on a linear stretch, and have been clipped at 50% of peak value to display structure in the wings. The right panel shows a radial slice through these functions. In this panel, $I(\vec{r})$ has been normalized to have a peak value of unity. The perfect OTF was formed from a simulated pupil mask of the Hale 5m, which accounted the shadows cast by the secondary and the four struts supporting it. These struts generate the fourfold symmetry apparent in the perfect OTF above. The transform $I(\vec{r})$ is the sum of the OTFs from the four objects in Figure 1, and the amplitude of $I(\vec{r})$ displays ringing that arises from interference among these different OTFs.
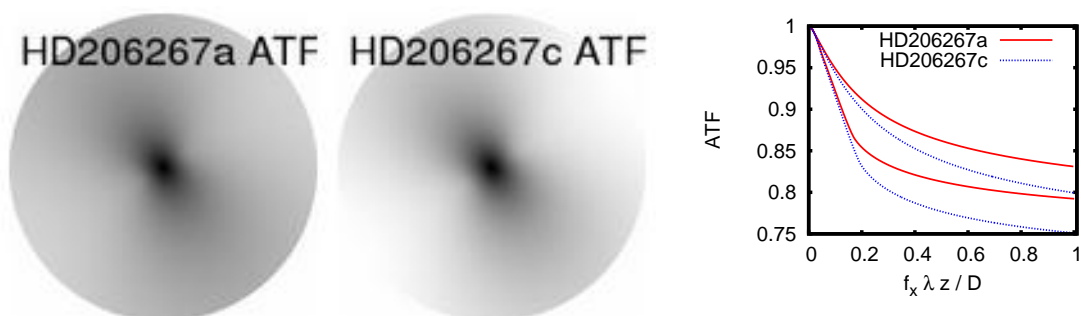

Figure 3. Anisoplanatic transfer functions (ATF) for HD206267a and HD206267c. In the absence of atmospheric turbulence, these functions would be unity everywhere. The ATF captures the effects of anisoplanatism, which degrades image quality by suppressing the optical transfer function in an anisotropic manner. This anisotropy gives rise to the familiar effect of radial elongation in the off axis AO PSF. The ATF for HD206267a is larger than that for HD206267c because it is closer to the guide star. The axes of symmetry in these functions are parallel and perpendicular to the vector connecting the source to the guide star. Radial slices along these axes are shown at far right for the two ATFs, with the higher curve corresponding to the perpendicular axis. These functions have been computed from Equation 3 using a turbulence profile measured contemporaneously by DIMM/MASS equipment operating at Palomar Observatory.

shown in this Figure. This OTF was formed using a model of the Hale 5m pupil that incorporated obscurations from the secondary mirror and its four support struts.

The anisoplanatic transfer functions for HD206267a and HD206267c computed from Equation 3 are shown in Figure 3. These transfer functions fall off more rapidly along the axis defined by the guide star and the source. It is this behavior that gives rise to the radial elongation that is a characteristic of the anisoplanatic PSF. A small evolution occurs in the transfer function between HD206267a and HD206267c due to the fact that the latter source is further from the guide star and suffers more anisoplanatic degradation.

These anisoplanatic transfer functions were used together with $OTF_{gs}(\vec{r})$ computed from the the guide star BD+56 2617C to perform the deconvolution. The results derived from this fit are shown in Table 1. These

	Differential Photometry	ρ (asec)	P.A. (deg)
BD+56 2617C	.153	11.77	119.26
HD206267b	.291	.098	232.56
HD206267c	.0125	1.80	318.70

Table 1. Differential photometry and astrometry determined by fitting the observation in Figure 1. These measurements have been quoted relative to HD206267a.
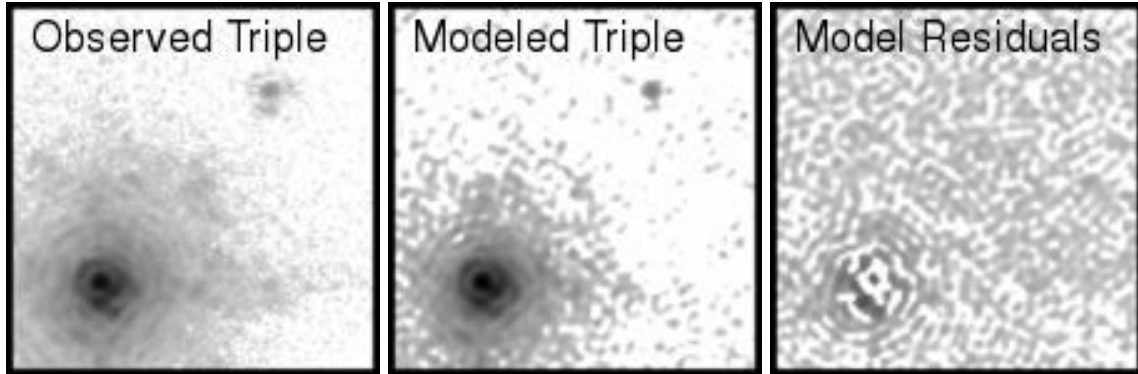

Figure 4. Observed, modeled and residual image of the triple system. The left panel shows the observation. The center panel shows a model of the observation formed from Equation 5 using the guide star OTF and the fitted parameters in Table 1. The right panel shows the difference between the model and the observation. The residuals are less than 5% of the peak value in the observed image.

results are quoted in terms of the differential photometry and astrometry relative to HD206267a.

The parameters derived in the fit were used together with the guide star PSF to construct a model of the triple system from Equation 5. This model is shown in Figure 4. Also shown are the residuals that remain after subtracting the model from the observation. These residuals have an amplitude less than 5% of the original observation, indicating that the fit has accounted for most of the signal. The modeled PSF of HD206267a was used to evaluate the Strehl ratio at the location of this star. The guide star Strehl ratio was 52%, and had fallen to 44% at this location due to the effects of anisoplanatism.

Lastly, the guide star OTF was derived from Equation 8 using the anisoplanatic transfer functions and the values of b_p and $\vec{\theta}_p$ determined in the deconvolution. This OTF and the corresponding PSF are shown in Figure 5. Repeating the fit using this refined OTF led to unrealistically small residuals in the vicinity of the close double. As indicated in Table 1, HD206267a and HD206267b account for most of the signal in the observation. This likely led to the artificial removal of noise in the vicinity of the close double. Under more general circumstances in which the observation is populated by many point sources, the OTF derived using this procedure may be of more utility.

6. CONCLUSIONS

The techniques described above constitute a practical method for the analysis of crowded field adaptive optics observations that extend beyond the isoplanatic patch. This formalism incorporates the field dependence of the PSF that arises from anisoplanatism into a χ^2 minimization procedure, with which the differential photometry and astrometry of stars within the field may be extracted. The preliminary results on HD206267 presented here have demonstrated the utility of the technique in fitting a close double. Additional data will be required to establish the accuracy of the measurements shown in Table 1.
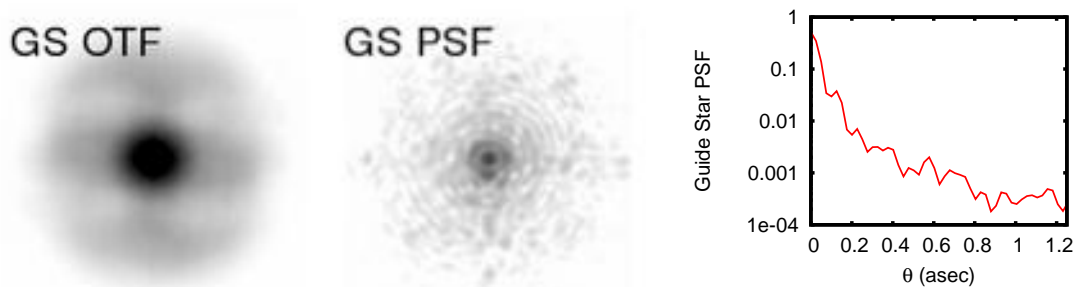
Figure 5. The guide star optical transfer function and point spread function determined from the observation in Figure 1. The guide star OTF has been determined from Equation 8 using the fitted values of b_p and $\vec{\theta}_p$, and the anisoplanatic transfer functions computed for each of these sources. The guide star PSF was formed by Fourier transformation of this OTF. A slice through the guide star PSF is shown in the right panel. This PSF has been normalized using the perfect diffraction limited PSF.

7. ACKNOWLEDGEMENTS

REFERENCES

1. S. M. Jefferies and J. C. Christou, "Restoration of Astronomical Images by Iterative Blind Deconvolution," *The Astrophysical Journal* **415**, pp. 862–874, Oct. 1993.
2. T. Fusco, J.-P. Véran, J.-M. Conan, and L. M. Mugnier, "Myopic deconvolution method for adaptive optics images of stellar fields," *Astronomy and Astrophysics Supplement Series* **134**, pp. 193–200, Jan. 1999.
3. E. Diolaiti, O. Bendinelli, D. Bonaccini, L. Close, D. Currie, and G. Parmeggiani, "Analysis of isoplanatic high resolution stellar fields by the StarFinder code," *Astronomy and Astrophysics Supplement Series* **147**, pp. 335–346, Dec. 2000.
4. M. C. Britton, "The Anisoplanatic Point Spread Function in Adaptive Optics," *Accepted by Publications of the Astronomical Society of the Pacific* , 2006.
5. R. N. Bracewell, *The Fourier Transform and Its Applications*, Boston : McGraw Hill, 2000.
6. T. Fusco, J.-M. Conan, L. M. Mugnier, V. Michau, and G. Rousset, "Characterization of adaptive optics point spread function for anisoplanatic imaging. Application to stellar field deconvolution," *Astronomy and Astrophysics Supplement* **142**, pp. 149–156, Feb. 2000.
7. W. H. Press, S. A. Teukolsky, W. T. Vetterling, and B. P. Flannery, *Numerical Recipes in C. The Art of Scientific Computing*, Cambridge: University Press, 1992.
8. M. Troy, R. G. Dekany, G. Brack, B. R. Oppenheimer, E. E. Bloemhof, T. Trinh, F. G. Dekens, F. Shi, T. L. Hayward, and B. Brandl, "Palomar adaptive optics project: status and performance," in *Proc. SPIE Vol. 4007, p. 31-40, Adaptive Optical Systems Technology, Peter L. Wizinowich; Ed.*, P. L. Wizinowich, ed., pp. 31–40, July 2000.

9. T. L. Hayward, B. Brandl, B. Pirger, C. Blacken, G. E. Gull, J. Schoenwald, and J. R. Houck, "PHARO: A Near-Infrared Camera for the Palomar Adaptive Optics System," *Publications of the Astronomical Society of the Pacific* **113**, pp. 105–118, Jan. 2001.

10. J. Vernin and C. Munoz-Tunon, "Measuring astronomical seeing: The DA/IAC DIMM," *Publications of the Astronomical Society of the Pacific* **107**, pp. 265–272, Mar. 1995.

11. V. Kornilov, A. A. Tokovinin, O. Vozyakova, A. Zaitsev, N. Shatsky, S. F. Potanin, and M. S. Sarazin, "MASS: a monitor of the vertical turbulence distribution," in *Adaptive Optical System Technologies II. Proceedings of the SPIE, Volume 4839*, P. L. Wizinowich and D. Bonaccini, eds., pp. 837–845, Feb. 2003.

12. W. Skidmore, M. Schöck, A. A. Tokovinin, G. Djorgovski, A. R. Walker, R. D. Blum, T. Travouillon, J. Seguel, E. E. Bustos, D. Walker, J. Vasquez, and P. E. Gillett, "The Thirty Meter Telescope site testing system," in *Proceedings of the SPIE, Volume 5489*, J. M. Oschmann, ed., pp. 154–164, Oct. 2004.